crystals

MDPI

Article

Electrical Control of Optical Liquid-Crystal-Guided Microstructures

Michal Kwasny and Urszula A. Laudyn *

Faculty of Physics, Warsaw University of Technology, Koszykowa 75, 00-662 Warsaw, Poland; michal.kwasny@pw.edu.pl
* Correspondence: urszula.laudyn@pw.edu.pl; Tel.: +48-22-234-72-77

Abstract: This work investigates nematic liquid crystal (NLC) optical guiding structures designed in typical sandwich-like NLC cells. With the support of an electrically controlled spatial topology of director orientation, we manage a linear and nonlinear light propagation with the realization of optical beam switching.

Keywords: nematic liquid crystals; electro-optical beam steering; optical waveguides and microstructures

Citation: Kwasny, M.; Laudyn, U.A. Electrical Control of Optical Liquid-Crystal-Guided Microstructures. *Crystals* **2022**, *12*, 325. https://doi.org/10.3390/cryst12030325

Academic Editors: Kohki Takatoh, Jun Xu and Akihiko Mochizuki

Received: 1 February 2022
Accepted: 23 February 2022
Published: 26 February 2022

1. Introduction

In most optical waveguide designs with external modulators, the optical switching is commonly realized through electro-optic, magneto-optic, all-optical, and thermo-optical effects [1]. The classic electro-optic (EO) effect is related to the refractive index alteration due to the modification of the index ellipsoid (or optical indicatrix) by applying an external electric field. Commonly used materials for electro-optic waveguides are $LiNbO_3$, $LiTaO_3$, $BaTiO_3$, electro-optic polymers, and nematic liquid crystals (NLCs) [1–6]. Due to the very high birefringence, combined with the possibility of changing it under the effect of external stimuli in thin-film NLC elements, the latter offers an excellent opportunity to develop novel methods and devices for the control of light beams [6,7]. The fluid nature of NLCs and their compatibility with most optoelectronic materials, polymers, and organic materials allow them to be easily incorporated with other elements in various configurations, forms, and geometries, thereby increasing the potential applications in novel photonic networks. NLCs are composed of rod-like molecules. Due to anisotropy in molecular structures, they exhibit electrical anisotropy. In a specific temperature range, called the nematic phase, long axes of molecules are approximately parallel to each other in. The averaged alignment direction defines a dimensionless unit vector $\boldsymbol{n}$ called the director. Most nematics are optically uniaxial and positive birefringent materials (with an extraordinary refractive index greater than the ordinary one, $n_e > n_o$) with an optical axis corresponding to the long axis of the molecules. The electric field oscillations are perpendicular and parallel to the direction of molecular orientation, and then an ordinary and extraordinary wave can be excited, respectively.

A standard configuration of the planar NLC cell that comprises two glass substrates and a liquid crystal layer is used. Light beams are directed perpendicular to the substrates. The transmission of light beams directed perpendicular to the substrates of the cell can be electrically controlled. Several optical types of NLC devices were demonstrated, using the linear properties of the material and electrical switching. The simplest example is the pixelated microdisplay (i.e., a spatial light modulator) for free-space beam shaping and steering [8]. Different possibilities are associated with the light beams reflected from the spatially modulated NLC structures. Spatially structured NLC cells are also used to transform linearly polarized light beams into beams with radial or azimuthal polarization [9]. In the last decades, another geometry in which the light beam propagates in the NLC layer along the glass substrates has also attracted considerable attention [10,11]. The concept of

NLC waveguide channels for polarization-independent light propagation was presented, and, for the first time, the concept and performance of a liquid-crystal-based electro-optical router was discussed. In addition to electro-optic and nonlinear effects that can be utilized for controlling the light propagation in photonic channels, the optical switching between waveguides can be realized using ferroelectric or smectic liquid crystals [10,12]. The presented waveguides consisted of an NLC infiltrated core made in PDMS channels. Such a configuration uses NLC in their isotropic phase for electro-optical-induced waveguides and supports polarization-independent light propagation [11]. Such NLC-waveguide architectures, as reported by the Fraunhofer IPMS [13], are based on a pure electro-optic approach. On the other hand, it has to be underlined that liquid crystal devices can also switch and route signals due to the modulation of external electric fields and the interplay between the light and molecules [14], especially when the nonlinearity of NLC plays a crucial role [15]. It has been shown in several papers that a milliwatt of power of laser radiation is sufficient for observation of the self-focusing effects and formation of the soliton-type propagation of light beams due to reorientation of the NLC director under an electromagnetic field of an optical wave [16–19]. Such soliton beams, called nematicons, form a waveguide channel in NLC film that can confine and guide the light beam. Two basic configurations can be distinguished: (i) Electro-optical, which combines initial reorientation under the external electric field with a huge nonlinear optical reorientation of the liquid crystal molecules, as well as the electrically induced reorientation of molecules with a substantial nonlinear optical response of the liquid crystal molecules. It can be realized by applying a voltage over a liquid crystal layer between a planar electrode and a thin stripe electrode [17,18]. (ii) Pure all-optical, which combines a proper initial boundary condition with nonlinear optical reorientation [20]. It is possible to perform all-optical switching and logic gating using only interactions between nematicons [21]. The possibility of confining a weak signal beam in the self-induced waveguide [22] opens the way to build novel optical interconnects for computing and communications. A few results of soliton manipulation have been proposed to control the soliton trajectory, e.g., the temperature [23,24] or initial boundary conditions [25,26].

This work utilizes light beam propagation in NLC media and demonstrates an electro-optical architecture that provides voltage control over the optical path. The operation principle of the presented device is based on the electrically controlled spatial topology of director orientation due to the reorientation of NLC molecules in the presence of a low-frequency electric field and specially designed electrode geometry. Our concept of reconfigurable optical microstructures supports the waveguiding of Gaussian beams in both linear and nonlinear cases, the latter in the sense of nematicons. In a linear case, an optical waveguide is induced by an electric field across the cell, within regions delimited by stripe, arch, or Y-shape electrodes. Simple waveguides are easily combined in more complex structures, including independently addressed electrodes providing light beam guiding, switching, and steering. In the nonlinear regime, we successfully demonstrate the complete electro-optical control by combining the electric response of NLC molecules with nonlinear light beam propagation in the sense of nematicons and utilizing the NLC cell with properly designed individually addressed electrodes over nematicons' trajectory. Both approaches can potentially obtain light-guiding structures in a planar geometry.

2. Materials and Methods

The basic waveguide structure of the electrically controlled NLC is shown in Figure 1a. It consists of two glass substrates, numbered 1 and 2, glued together with a specific distance. On the first substrate, there is a transparent indium/tin oxide electrode. On the second one, metallic electrodes of different sizes and shapes are prepared by the electron beam lithography (EBL) technique. The preparation of the electrodes is a two-stage lift-off process. Initially, a 200 nm thin poly(methyl-methacrylate) layer (PMMA 495K) is spin-coated on the clean glass substrate. After evaporation of the solvent, an additional gold layer is deposited on the surface of the polymer. This step is essential because a thin layer of gold

ensures the electrical discharging of the sample exposed on a focused beam of electrons, which irradiates the target shapes for the electrodes. Before the development process (in 1:3 solution of methyl isobutyl ketone:2-Propanol), a gold layer is removed by immersing the sample in KI_3 gold etchant (Sigma-Aldrich, St. Louis, MI, USA) and deionized water. The next stage of the process concerns subsequent metallization with a 10 nm underlay of Titanium and a 100 nm layer of gold. A final result is a glass substrate with deposited gold electrodes in designed shape and dimensions.

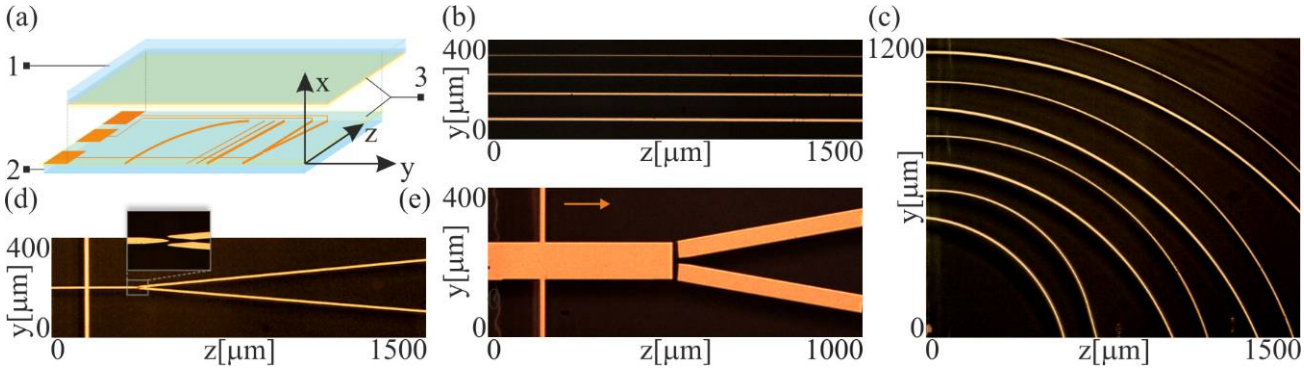

Figure 1. Electrically controlled NLC structures: (**a**) sketch of the NLC cell; (**b**) straight and (**c**) curved electrodes (widths 5 μm and 10 μm); (**d**) combination of three independently controlled electrodes for realizing optical Y-junction (10 μm width, one input and two output ports); (**e**) combination of Y-shaped independently controlled electrodes (the widths 100 μm and 50 μm) for the realization of beam switching in nonlinear propagation regime (a nematicon).

Whenever required, the additional polymeric layer (number 3, Figure 1a) can be spin-coated on the substrates on the top of the electrodes and their surrounded areas and rubbed to ensure the initial planar orientation in the desired direction. Such prepared glass substrates are then used for cell preparation. The cell thickness equals 12 and 30 μm for linear and nonlinear beam propagation, respectively. A small amount of NOA-61 UV-curing photopolymer mixed with 12 or 30 μm glass spacers is placed over one substrate. The counter substrate is put over it, and after proper alignment, the photopolymer is cured by exposing it to ultraviolet light. Because of the relatively small cell thickness used for linear beam propagation and electro-optical waveguide formation, no additional interfaces limiting the outflow of NLC were used, yet no adverse effects related to NLC leakage or meniscus formation were observed. The NLC cells that are made contain electrodes to realize the electrically induced waveguides for the light beam propagation and switching between two output ports. Prepared structures are shown in Figure 1b (straight electrodes), Figure 1c (bend electrodes), and Figure 1d ("fork" electrode), and they are designed to operate in a linear optical regime, i.e., when the intensity of the propagated beam is not high enough to cause additional reorientation of the molecules. The width of the electrodes is 5 and 10 μm; the length of the electrodes is 4 mm (straight); 0.5–1.5 mm (bend); 0.35 mm (the length of the input electrode of the fork structure); and 1.2 mm is the length after forking. The minimal distance between electrodes is 3 μm.

For nonlinear beam switching, an NLC cell with one electrode of a 100 μm width and 500 μm length and two output electrodes of a 50 μm width, 500 μm length and minimal separation of 10 μm is used, as shown in Figure 1e. This cell contains a rubbed alignment layer that anchors molecules of NLC along the *z*-axis.

The assembled cells are filled up with NLC by capillarity, taking care to avoid bubbles/gaps near the boundaries, and examined under a polarization microscope to verify the proper alignment of the director. As an NLC material, a typical-birefringent 6CHBT nematic liquid crystal is used: characterized by positive dielectric anisotropy ($\Delta\epsilon = 0.42$ at 1 kHz); refractive indices: $n_o = 1.4967$, $n_e = 1.6335$ at λ = 1064 nm and $n_o = 1.52$, $n_e = 1.68$ at λ = 532 nm (at room temperature); the Frank elastic constants are K_{11} = 8.96 pN;

K_{22} = 3.61 pN; K_{33} = 9.71 pN (for splay, twist and bend, respectively); and the nematic–isotropic phase transition temperature is T_c = 43 °C [27].

Figure 2a presents the basic experimental setup used for beam propagation analysis. As an input, we used the linearly polarized (along the *x*-axis) Gaussian beam (TEM_{00}) propagating along the *z*-axis. The beam is focused in the cell midplane (a beamwidth w_0 = 2.5 µm) at the input of the cell (z = 0). The first CCD camera visualized the beam evolution along z in the principal *yz*-plane by imaging the light scattered out of the plane, while the second CCD camera is used to visualize the beam profile in the *xy*-plane at the output. The position of the sample is adjusted by the precise three-axis micro-translation stage in the *x*, *y*, and *z*-direction. A low-frequency (1 kHz) sinusoidal waveform generator combined with a signal amplifier drives NLC molecules and induces out-of-plane reorientation.

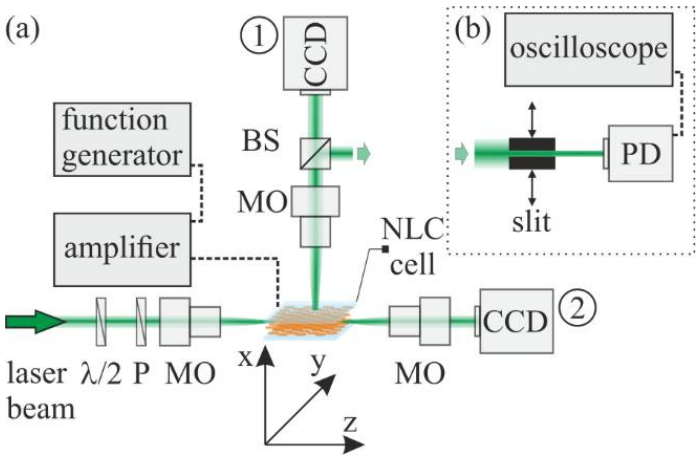

Figure 2. Sketch of the experimental setup showing: (**a**) part devoted to beam coupling and visualization of the beam propagation; (**b**) part for determining waveguide formation times. λ/2—halfwave plate, P—polarizer, MO—microscope objective, BS—beam splitter, CCD—digital camera, PD—photodiode.

To measure the formation times of waveguides induced by straight electrodes, a part of light collected by the first CCD camera is redirected to the photodetector (PD), schematically presented in Figure 2b. The amplitude of the electric signal recorded by the oscilloscope is proportional to incident light intensity. Without driving voltage applied to the electrodes of the NLC cell, the beam diffracts; therefore, a weak electric signal (mostly noise-related) is recorded by oscilloscope. When the beam is propagated within a waveguide, some light is scattered out of the propagation plane. Then, the light is collimated by the microscope objective reaching the photodiode. Therefore, an electric signal corresponding to a high state is recorded. To increase the dynamic range between a high and a low state, a mechanical slit that clips part of the beam is used.

On bare glass and metallic surfaces, NLC molecules are oriented randomly (in-plane, *xy*-plane); however, they remain parallel to the glass surface [28]. Under the influence of an external electric field (along the *x*-axis), NLC molecules (with positive dielectric anisotropy) start to reorient (out of plane, along the *x*-axis) and align along the electric field, i.e., towards homeotropic texture. This means that the initial molecular alignment (orientation in *xy*-plane) is not necessary to induce NLC waveguides (for TM-polarized beam) using an external electric field, as already presented by Fraunauhoffer [13]. In our work, the impact of alignment layers on electro-optically induced NLC waveguides was analyzed (e.g., driving voltages, formation times). In both configurations of NLC cells, the waveguide formation times and the driving voltages are comparable.

3. Results

3.1. Linear Waveguides

The light guiding within an electrically induced and controlled NLC waveguide is based on total internal reflection from two regions within the NLC layer with a different spatial distribution of the molecules [13,14,29]. When there is no voltage applied, the NLC molecules are uniformly oriented in a planar configuration (along the *z*-axis) over the whole volume of the sample. As the voltage increases (above the Freedericksz threshold value), molecules reorient out of plane towards the electric field lines to homeotropic orientation. Figure 3a presents the orientation of molecules in a uniform NLC cell characterized by the planar molecular alignment of a thickness equal to 12 μm, the same as the thickness of the analyzed NLC structures. The reorientation is induced by a uniform electric field; however, the final position of molecules depends, among others, on anchoring conditions, liquid crystal elasticity and applied voltage, as it is sketched for 6CHBT NLC for U = 1.2 V— black square, 1.5 V—gray circle, 2.0 V—light gray triangle, 2.5 V—magenta hexagon, 7.0 V—violet hexagon, and 20.0 V—purple star. As the molecules reorient out of plane, the refractive index for the input beam linearly polarized along with x increases according to $n_e(\theta) = n_o n_e / (n_e^2 \cos^2\theta + n_o^2 \sin^2\theta)^{-\frac{1}{2}}$, where: θ is the angle between the long axis and yz-plane, and n_0 and n_e are ordinary and extraordinary refractive indices, respectively, as is plotted in Figure 3b. In contrast, in the regions without electrodes, molecules maintain a planar orientation. Therefore, in a non-uniform electric field induced by structured electrodes, a transverse modulation of the refractive index is obtained. NLC cells with structured electrodes resemble a graded waveguide structure for a linearly polarized input beam with TM (along with x-axis) polarization.

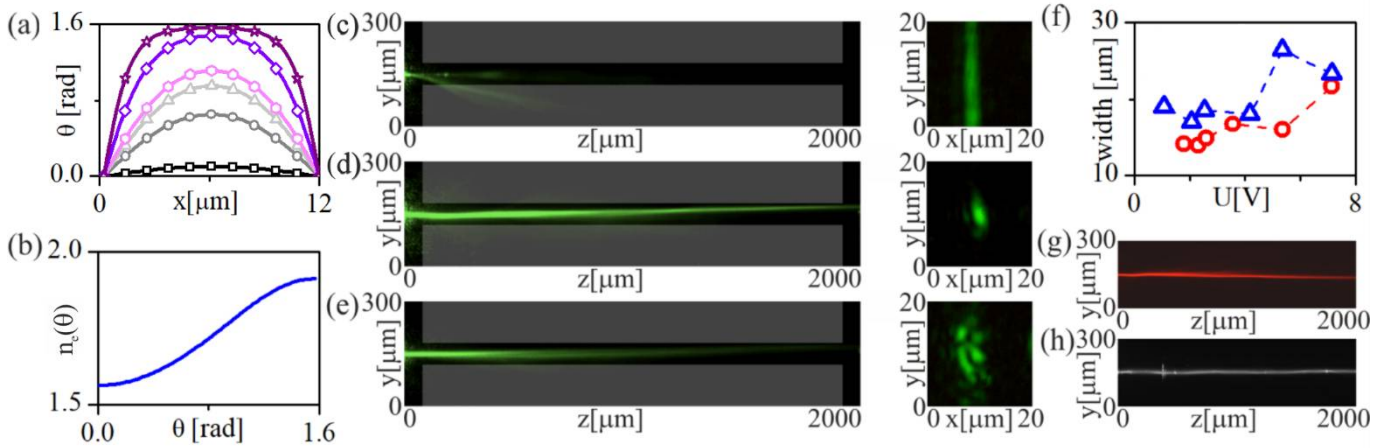

Figure 3. (**a**) Director distribution in NLC cell along the x-axis (cell thickness) as a function of the voltage (solid lines), plotted for U = 1.2 V—black (square), 1.5 V—gray (circle), 2.0 V—light gray (triangle), 2.5 V—magenta (hexagon), 7.0 V—violet (diamond), and 20.0 V—purple (star). (**b**) Refractive index for TM-polarized beam (λ = 532 nm) as a function of the orientation of molecules. (**c**–**e**) Experimental evidence of a (1D + 1) waveguide formation (electrode width 5 μm) and propagation of TM-polarized beam at λ = 532 nm. Beam evolution in yz-plane (left panel) and corresponding output profiles in xy-plane (right panel) (**c**) for U = 0 V, (**d**) for U = 2.3 V, and (**e**) for U = 7.0 V biasing voltage. (**f**) Mean beam width plotted for different voltages for 5 μm (red circles) and 10 μm (blue triangles) electrode widths. (**g**) Propagation of a TM-polarized beam at λ = 642 nm and (**h**) λ = 1064 nm, for U = 1.8 V and 5 μm electrode width.

Without an electric field, the NLC molecules maintain planar orientation $(\theta = 0^0)$ and the TM-beam propagates along the z-axis and diffracts as it does in isotropic media, with the refractive index n_0. For a driving voltage above the Freedericksz threshold value, the molecules reorient under the electrode, increasing the angle θ. As a result, the refractive index for the TM-polarized beam increases, and a waveguide channel is formed.

The laser beam propagation in the designed structure with a straight electrode is shown in Figure 3c–e. The linearly polarized input beam along the x-axis beam at λ = 532 nm is launched into the NLC sample in the region of the stripe-shaped electrode. Without the external voltage (U = 0), the light beam diffracts, increasing its width with propagation distance (Figure 3c). In the output plane (xy), this is visible as a broad illuminated region along the y-axis, confirming the beam diffraction in the yz-plane. Along the x-axis, the beam does not diffract significantly due to its limited thickness. Applying a voltage of (U = 2.3 V) causes a reorientation of the NLC molecules and thus an increase in the refractive index in this region, which consequently leads to the excitation of the waveguide channel (Figure 3d). The intensity distribution at the cell output is approximately Gaussian, characterized by partial ellipticity. The approximate diameter of the modal field is $w_x \cong 1.8$ µm and $w_y \cong 2.9$ µm, measured as FWHM values. Increasing the voltage up to 7 V widens the waveguide in both x and y directions due to further reorientation and saturation, and nonlocality of NLC molecules, respectively (Figure 3e). The beam output profile becomes irregular and corresponds to a mix of higher-order guiding modes. Therefore, the induced waveguide starts to support more and more higher-order modes.

The mean width of a beam as a function of biasing voltage on electrodes of a width equal to 5 and 10 µm is plotted and presented in Figure 3f. The beam is the narrowest for a biasing voltage of about 2 V, then, as the voltage increases, the mean width of a beam increases as well. Biasing voltage of 7 V results in irregular optical field distribution at the output. It indicates that propagation is realized as a superposition of higher-order modes.

An electrically induced waveguide also supports different wavelengths. The propagation of the visible beam at λ = 642 nm (Figure 3g) and infrared one λ = 1064 nm (Figure 3h) is recorded for a U = 1.8 V biasing voltage. Furthermore, NLC waveguides are not limited to straight geometry. An example is presented in Figure 4, where there are sketched arch-shaped electrodes of different sizes (left panel, Figure 4a) and a combination of three arch electrodes (left panel, Figure 4b). The propagation of a TM-polarized beam of a wavelength λ = 532 in a single arch-shaped channel and beam splitting at three different combined NLC arch-shaped electrically induced waveguides (driving voltage U = 2.3 V) are shown in Figure 4a,b (right panels). The possibility of beam splitting between more guiding channels makes it possible to design and perform novel photonics devices for integrated optical circuits.

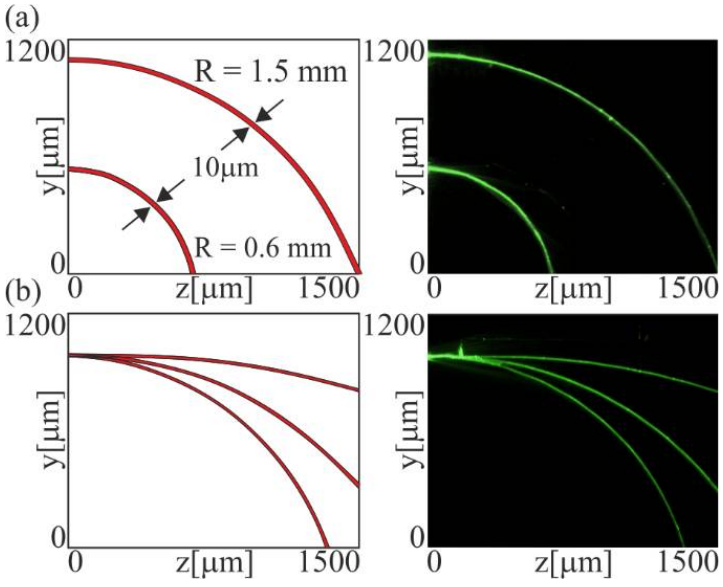

Figure 4. (**a**) Scheme of the curved geometry of the electrodes in NLC cell (left panel) and λ = 532 nm, TM-polarized beam propagation (right panel). (**b**) Combined three arch-shaped electrodes (left panel) and TM-polarized beam propagation at λ = 532 nm for U = 2.3 V.

3.1.1. Waveguide Formation Times

One of the important issues and also one of the significant drawbacks is the dynamics of the waveguide channel formation. Due to the fact that reorientation involves, in general, the rotation of the molecules, it is a relatively slow process. The relationship between the response time and the dynamic rotational viscosity γ and the cell thickness d is directly proportional: $t_r \sim \gamma d^2$. From this relation, the larger the dynamic rotational viscosity, the slower the response time, but the thickness is even more critical in determining the response time, as it is squared with the response time, which can be defined as the time that a certain region of an NLC cell takes to turn from on to off or vice versa. NLC with a low rotational viscosity favors a rapid switching using an electric field. For a specific NLC, the value of the viscosity cannot be changed freely; however, the electrical driving signal can be optimized to maximize the overall performance of the structure. In order to determine the formation time of the induced waveguide structure, the setup, as shown in Figure 1b, is used. The waveguide formation time is defined as the time from the moment the voltage is switched on until the transverse beam profile at a given propagation distance does not change and is more or less the same as the input beam profile. In an experiment, a more convenient way is to use a photodetector at the output of the waveguide. The criterion for the waveguide formation time that is measured is a time from beam coupling to the input to a moment when the electric signal at the photodetector reaches 0.9 times its maximum value. Generation of a waveguide channel requires a voltage just above the Frederiks threshold value. Such a voltage value forces the molecules to reorient, thus providing a change in refractive index $(n_e(\theta))$ sufficient to guide the light beam. However, in this case (relatively small voltage value), the reorientation time of molecules is on the order of hundreds of milliseconds (for the 12 µm thick cell).

The obtained NLC waveguide formation times are presented in Figure 5a. The reorientation time is estimated from a sequence of images taken by a CCD camera operating at a recording rate of 30 fps, i.e., the measurement resolution is 33 ms. No significant differences are observed in NLC cells with and without alignment layers at the bottom and top surfaces. However, the arrangement of all molecules towards the propagation direction seems to be a better approach to the reorientation process and slightly increases the response times of the molecules.

The reorientation rate directly depends on the amplitude of the driving voltage. For a driving voltage with an amplitude higher than the threshold value, the reorientation process occurs significantly faster than for voltages of the order of the threshold value. On the other hand, as shown already in Figure 3a, higher voltages are disadvantageous because they induce too high reorientation (and thus a change in refractive index) and promote/support higher-order modes. Therefore, we propose a solution of using two voltages: a high overdrive voltage to achieve fast molecule reorientations and a voltage to ensure single-mode waveguide maintenance. The duration time of this high amplitude driving voltage must be precisely determined. It is important to reduce the amplitude of a voltage to the optimum value needed for waveguide formation at a specific time. An overdriving voltage duration that is too short will not result in a sufficient reorientation angle to induce waveguide formation. On the other hand, when the duration of the overdriving voltage is too long, the molecules will reorient too much, and the induced waveguide becomes highly multimodal.

To determine the overdrive voltage duration, a typical configuration with two crossed polarizers and a planar NLC cell with the optical axis oriented at 45° to the polarizers' axis is used. Without an electric field, an NLC cell placed between crossed polarizers acts as a wave plate and brightens the field of view. As the voltage is switched on, the molecules start to reorient, and the phase delay between ordinary and extraordinary wave components changes. As a result, the intensity of a beam transmitted through the optical system varies in time. It stabilizes at a certain level depending on the final position of the molecules for a given voltage. Transmitted light intensity reaches the successive minima and maxima,

finally reaching zero for the entirely reoriented molecules almost to a homeotropic texture. The number of oscillations increases with the NLC birefringence and cell thickness.

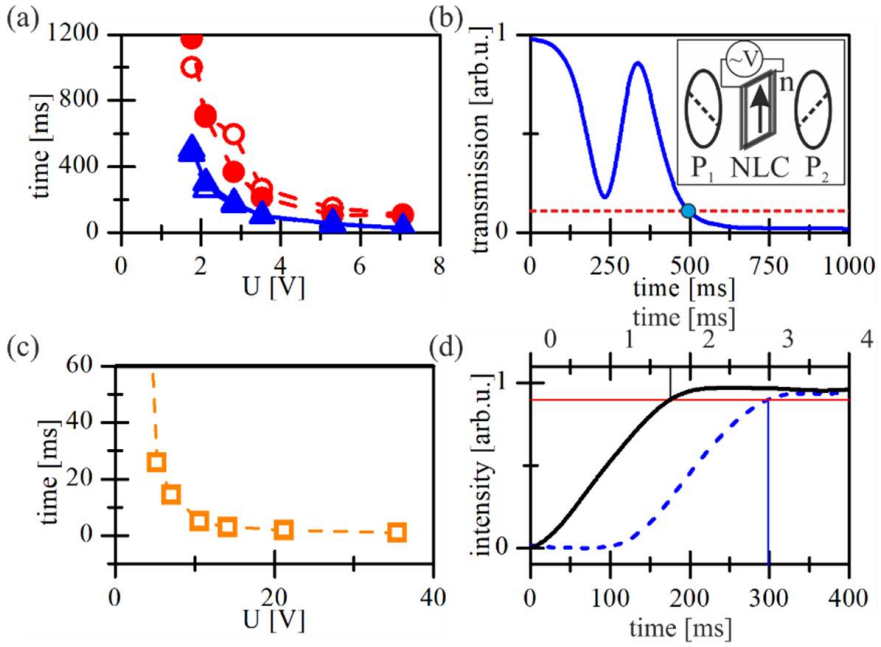

Figure 5. Experimental results on waveguide formation times and reorientation times. (**a**) Formation times as a function of voltage for 5 μm (red circles) and 10 μm (blue triangles) electrode widths. Open and filled markers refer to cells without and with an additional alignment layer, respectively. (**b**) Transmission through NLC cell vs. determined in the cross-polarizer configuration plotted for U = 2.1 V. The dotted red line denotes a decrease in the transmitted beam intensity to 10% of the maximum value. (**c**) Reorientation time as a function of a biasing voltage (orange squares). (**d**) Comparison of waveguide formation times for biasing voltage U = 2.1 V with (solid black line) and without 21.2 V overdriving voltage (dotted blue line). Intensity represents voltage rise time on the photodetector.

The oscillatory character of these changes for U = 2.1 V (the voltage value for which single-mode waveguide is formed) is presented in Figure 5b. In the measurements intended to determine the duration time of high overdriving voltage, a reorientation time is defined as the time from when the voltage is turned on until the intensity of the transmitted beam reaches 0.1 times its maximum value. From this, the reorientation times are determined for different overdriving voltages and plotted in Figure 5c. The line fitted to the experimental data is exponentially decreasing, and further increasing the voltage above a few tens of volts does not significantly reduce the reorientation time.

The waveguide induction time measurements are investigated as a function of overdriving voltage of duration, and amplitude presented in Figure 5b. The experiment is performed in the same experimental setup as in Figure 2a. A sinusoidal overdriving voltage of frequency 10 kHz and a precisely determined duration and amplitude, after which the voltage dropped to a value of U = 2.1 V, are applied to the NLC cell. The waveguide formation time is defined as the time that elapses from the voltage on until the electric signal generated on the photodetector reaches 0.9 times its maximum.

The application of a high overdrive voltage made it possible to shorten a switching time by two orders of magnitude. The best result is obtained for U_{ovr} = 21.2 V, and the formation time corresponds to 2.2 ms. The impact of a short duration voltage with high amplitude (2.2 ms; 21.2 V) is presented in Figure 5d.

3.1.2. Splitting Structures

Since the beam trajectory coincides with the shape of the electrodes, it is possible to design more complex electro-optical circuits designed for optical switching. The Y-splitter design is the simplest element to implement light splitting or switching. Figure 6a shows a top view image of the designed Y-splitter. It consists of three individual electrodes with a width of 10 μm each, namely, (1), (2) and (3), as marked on the photo, which allows for independent voltage control in each branch. The length of the first electrode to the forking (splitting) is equal to 600 μm; the angle between the second and third electrode is equal to 7° and the length of these electrodes is equal to 600 μm; thus, the distance between the output electrode (the "fork" width) is 50 μm. The voltages applied to the input electrode and two output electrodes are labelled as U_1, U_2, and U_3, respectively. The visible dark stripe perpendicular to the input electrode is used to supply the voltage and does not affect the beam propagation.

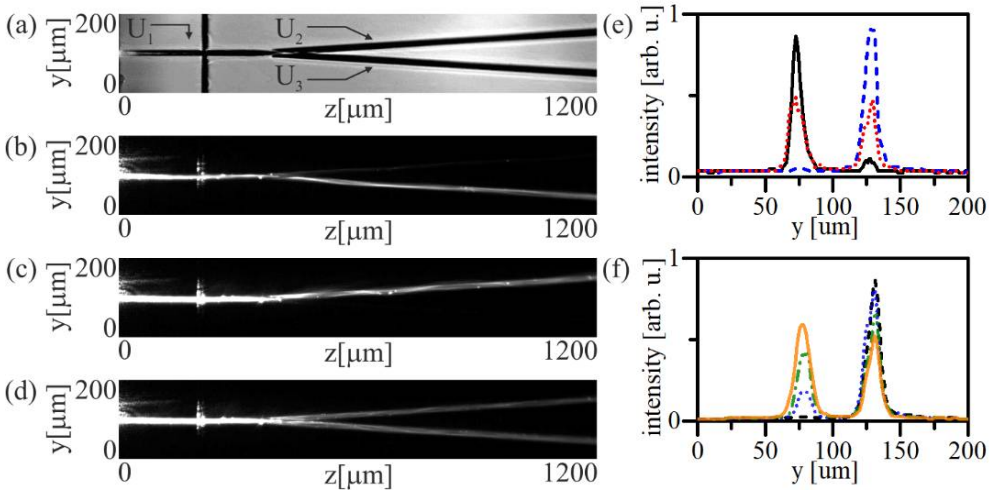

Figure 6. Electro-optic structure with three independent electrodes (with a width of 10 μm each) that forms an optical Y-junction for TM-polarized beam: (**a**) Photo of the designed structure illuminated by white light. (**b**–**d**) Beam propagation at λ = 1064 nm and (**e**) intensity cross-sections along the *y*-axis at z = 800 μm that corresponds to biasing voltage of 2.1 V applied to the electrodes: no. 1 and 3 (solid black line), no. 1 and 2 (dashed blue line) and no. 1, 2 and 3 (dotted red line), respectively. (**f**) Intensity cross-sections along the *y*-axis at z = 800 μm in case of biasing voltage of 2.1 V applied to electrodes 1 and 2, as a function of voltage at electrode no. 3: 0 V (dashed black line), 1.0 V (dotted blue line), 1.4 V (dash-dotted green line), 2.1 V (solid orange line).

Figure 6b–d shows the propagation result of linearly polarized TM infrared beam λ = 1064 nm in the fabricated structure. The first electrode, supplied with a voltage U_1 = 2.1 V is used to induce the input channel. Applying a voltage to the top electrode (U_2 = 2.1 V; U_3 = 0 V) induces the upper channel and the beam follows the direction (Figure 6b), while applying a voltage to the third electrode (U_2 = 0 V; U_3 = 2.1 V) switches the beam into the lower channel (Figure 6c). Applying the same voltage to all three electrodes ($U_1 = U_2 = U_3$ = 2.1 V) excites three waveguide channels in the medium, and the laser beam propagates along these channels (Figure 6c). The light is captured by a single input waveguide and then undergoes splitting/forking with approximately equal intensities due to the electrode geometry. Figure 6e,f shows the corresponding intensity distribution in the lower and upper channels at a distance of 800 μm for different voltages, illustrating the principle operation of the structure.

3.2. Nonlinear Waveguides

In a nonlinear case, an intense light beam in an NLC medium can propagate with a constant width at a propagation distance exceeding the Rayleigh range multiple times. For

the TM-polarized beam, the generation of nematicon requires proper alignment direction. The strongest nonlinear response of the molecules is when molecules are oriented in the direction of the **k** vector. For a non-threshold reorientation of molecules in the presence of a light beam and avoiding the Freedericksz threshold effect, the initial pretilt of molecules is induced by an external electric field (Figure 7a). Without an electric field, molecules are subjected to a threshold, and, for the TM-polarized beam, diffraction is observed (Figure 7b). In the presence of an electric field, molecules tend to reorient towards the x-direction. The beam propagates in the form of spatial soliton (nematicon) and preserves its width at a distance of a few millimeters (Figure 7c).

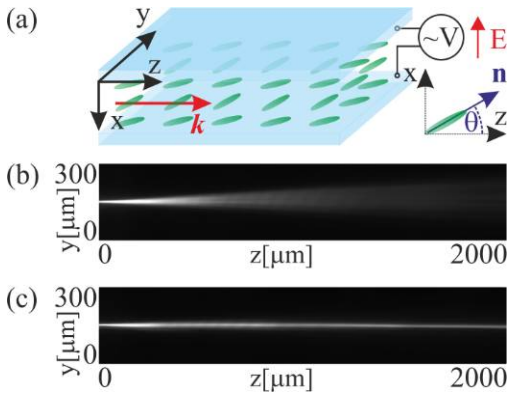

Figure 7. Experimental evidence of the light beam propagation in 6CHBT NLC cell, (λ = 1064 nm; optical power P = 1.5 mW): (**a**) The geometry of a cell and molecular orientation induced by an electric field of amplitude above the threshold value. (**b**) Diffraction observed in a *yz*-plane for beam propagation without biasing voltage. (**c**) Nematicons propagation for U = 1.6 V.

As described in the introduction part, in the nonlinear case, a light beam with sufficiently high intensity can propagate in NLC medium, with a constant width over distances many times the Rayleigh range, in the form of a so-called nematicon.

The alignment layers ensure planar orientation in the *yz*-plane with initial molecular anchoring at $\theta = 0$ with respect to the *z*-axis (Figure 7a). Indium/tin oxide (ITO) thin transparent electrodes deposited on the inner side of the NLC cell are applied to provide an adjustable low-frequency electric field for the out-of-*yz*-plane reorientation of the molecules. The NLC cell under consideration has been infiltrated with 6CHBT NLC and the linear polarized TM (along *x*-axis) light beam at λ = 1064 nm with optical power P = 1.5 mW has been focused to the waist of several micrometers and then launched into the NLC cell with its k vector oriented along the *z*-axis, as schematically presented in Figure 7a. Figure 7b presents an experimental photo of light beam propagation without an external electric field. As one can clearly see, the light beam diffracts. Without an external electric field, the reorientation is subjected to a threshold value much higher than the 1.5 mW. When a sufficiently high voltage is applied to the ITO electrodes, the NLC molecules are reoriented in the *xz*-plane, changing, thus, the director orientation. Indeed, by applying an electrical bias of 1.6 V (1 kHz), the self-trapped beam of TM-polarization is induced (Figure 7c). The beam propagates in the form of a nematicon and preserves its width at a distance of 2 mm.

Among other possibilities of controll light propagation in NLC structures [30–33], bycombining the propagation of the nematicon with the properties of structures with specially designed electrodes as described in Section 3.1, we obtain a configuration for changing the propagation direction of the nematicon in a Y-shaped geometry, as presented in Figure 8a. It is composed of one initial electrode of a width of 100 μm and two electrodes of a thickness equal to 50 μm with a short gap between them. The width of a cell is 50 μm. The amplitude of the driving voltage on each electrode can be controlled independently. The propagation direction of the nematicon between the upper (U_1) and lower (U_2) electrodes can be change by applying the voltage to the proper electrodes. To generate nematicon in

the area designated by the initial electrode (U_0), a TM-polarized IR beam of initial width w_0 = 2.5 µm and optical power P = 1.5 mW is coupled to the middle part of the NLC cell. For the biasing voltage, the U_0 = 2.1 V beam forms a nematicon that propagates along the z-axis. Depending on the voltages U_1 and U_2, a nematicon is redirected to the upper or lower part of the NLC cell, as presented in Figure 8b,c. Trajectories of the nematicon that propagates in the case of U_0 = 2.1 V and U_1 = 2.1 V or U_2 = 2.1 V are plotted in Figure 8d. After propagation over a 1 mm distance, the spatial separation of a beam exceeds 300 mm, which may be advantageous for the application of the structure in integrated optical circuits. More NLC cells can be combined to obtain guiding/switching structures or decouple the beam from the NLC cell.

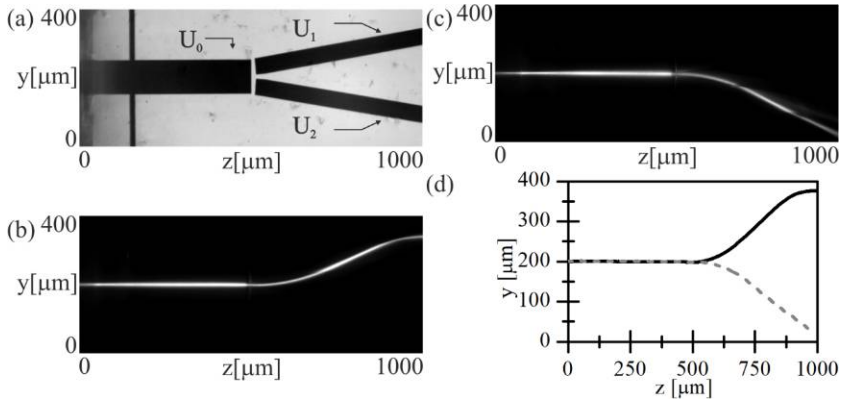

Figure 8. Combination of three independent powered electrodes of a width of 100 and 50 µm that formed an optical Y-junction for TM-polarized beam: (**a**) Electrodes within NLC cell. (**b**) Nonlinear propagation of a beam at λ = 1064 nm and optical power P = 1.5 mW for biasing voltage of $U_0 = U_1$ = 2.1 V and (**c**) $U_0 = U_2$ = 2.1 V. (**d**) Corresponding to (**b**,**c**) beam trajectories—black solid to light gray dashed line, respectively.

4. Perspectives

Expanding the structure by the additional electrode/electrodes can increase the number of output ports. The 1 × 3 Y-switching structure was prepared by the same method as the previously described 1 × 2 Y-shaped optical switches and is presented in Figure 9. It consists of four independent electrodes, one of which is devoted to inducing the pretilt of molecules in an initial channel, and the other three are responsible for changing the direction of nematicon propagation between upper (U_1), middle (U_2), and lower (U_3) output ports. Figure 9b shows a low-power signal beam (λ = 532 nm, TM-polarization) propagation, the width of which increases along with propagation distance. For a high-power TM-polarized beam (λ = 1064 nm, P = 1.6 mW) and driving voltage U_0 = 1.7 V, a nematicon is formed. A nematicon can be routed between three output ports depending on U_1, U_2, and U_3 driving voltages, as it is plotted in Figure 9c and shown in Figure 9d–f. A low-power co-polarized signal beam co-coupled with a high-power IR beam follows the nonlinearly induced waveguide channel presented in Figure 9g–i.

An interesting advantage of the proposed configuration is that the signal can be switched between the output channels not by changing the voltage value, but by using the phase shift of a sinusoidal electrical signal on the electrodes. A structure is analogous to the one described above and is shown schematically in Figure 10a. Based on the numerical calculations (presented in Figure 10b), it is seen that there is a considerable asymmetry in molecular reorientation out of the *yz*-plane in the proximity of the forked area when the out of phase electrical sinusoidal signal is applied to the upper electrode. In the qualitative numerical results, a theoretical value of reorientation angle in a cell midplane was found by solving the Euler–Lagrange equation, with the assumption of strong anchoring conditions at the boundaries (a planar alignment with an initial orientation of molecules at $\theta \cong 0$): $K_{11}\frac{d^2\theta}{dx^2} + \frac{1}{2}\varepsilon_0\Delta\varepsilon E^2 \sin 2\theta = 0$, where K_{11}—the splay elastic constant; E—amplitude of the

electric field (above the threshold value) directed along the *x*-axis; Δ*ε*—dielectric anisotropy; *θ*—reorientation angle of molecules out of the *yz*-plane. The voltages included in the calculation are $U_0 = U_2 = 2.0$ V. For the sake of simplicity, the counter phase of the voltage on the upper electrode is assumed to be $U_1 = -2.0$ V. In the considered situation, the reorientation of the molecules is asymmetric about the symmetry axis of the electrodes in the *z*-direction. Consequently, only one direction of nematicon propagation is preferred, resulting in switching the nematicons trajectory from the upper channel (when all-electrical signals are in phase) to the bottom channel (when the electric signal at the top electrode is out of phase with the others).

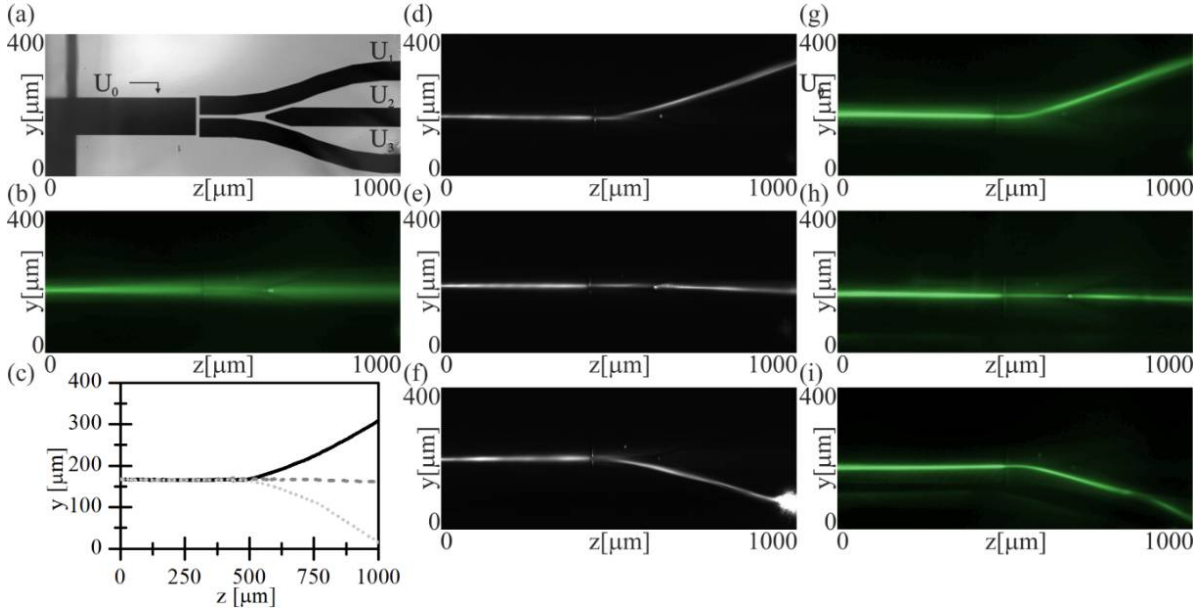

Figure 9. Combination of four independent controlled electrodes of a 100 μm width in the initial channel and 50 μm in the output channels formed an optical 1 × 3-junction for TM-polarized beam: (**a**) Electrodes within NLC cell. (**b**) Propagation of low-power signal beam (λ = 532 nm, TM-polarization). (**c**) Trajectories of self-induced nonlinear waveguides obtained for IR beam of optical power P = 1.6 mW, TM-polarization, $U_0 = 1.7$ V. (**d**–**f**) Nematicon propagation for driving voltage applied sequentially to the electrodes $U_1 = 1.7$ V, $U_2 = 1.7$ V and $U_3 = 1.7$ V. (**g**–**i**) Guided low-power signal beam (λ = 532 nm, TM- polarization) co-coupled collinearly with an infrared beam.

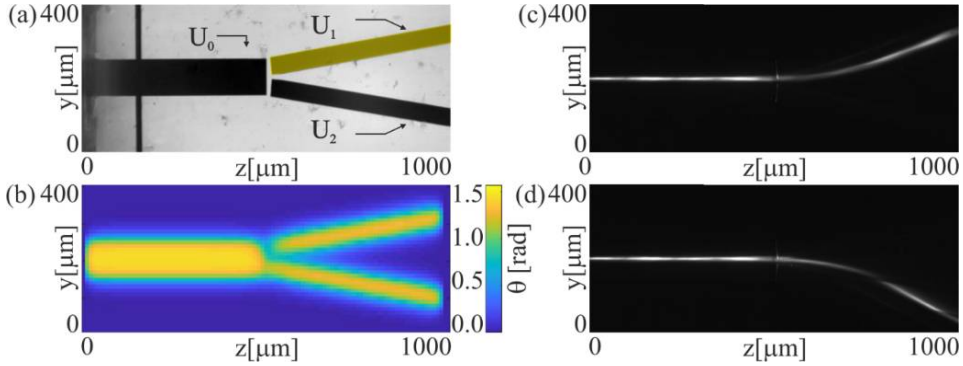

Figure 10. Redirection of nematicon in an optical Y-junction for TM-polarized beam using the phase shift of a driving voltage: (**a**) Electrodes within NLC cell, with a marked one with variable phase. (**b**) Asymmetry in the out-of-plane molecular reorientation when sinusoidal signal U_1 is out of phase with the U_0 and U_2 of the electrical signals—numerical calculations. (**c**) Experimental nonlinear beam propagation of a wavelength λ = 1064 nm and optical power P = 1.5 mW in case of $U_1 = 1.7$ V remains in phase and (**d**) out of phase to U_0 and U_2.

Experimental results presenting beam propagation and trajectory switching between two electrically induced channels due to a counter phase driving signal on the upper electrode (U_1) are presented in Figure 10c,d. The voltages of the sinusoidal signal (1 kHz) were $U_{0,1,2}$ = 1.7 V. A phase delay between the electric signal on the upper electrode (U_1) was varied, ranging from 0 to π. When all voltages remain equal, and in phase, the distribution of the effective refractive index for the TM-polarized IR beam in the forking section of the NLC cell is symmetrical, and the initial beam propagation direction is such that the beam propagates in the upper channel—Figure 10c. When the electric signal (U_1) was delayed by π, the effective refractive index in the area between electrodes in the initial part of a structure (U_0) and the upper one (U_1) decreases, and the beam propagation switches to a lower channel—Figure 10d. The optical power of a beam remains constant in both cases at P = 1.5 mW.

5. Conclusions

In this paper, electrically induced optical waveguides based on liquid crystals for a linearly polarized light beam have been presented. They operate by refractive index change induced by the reorientation of molecules under the influence of an external slowly varying electric field. Different geometries, both straight and curved waveguide structures as well as Y-shaped switches, have been presented. A method that significantly reduces the formation time of such waveguides (single milliseconds) has been proposed, which is undoubtedly an important step towards applications.

In the case of waveguides induced using both an external electric field and beam intensity (nonlinear case), independently controlled electrodes with a given geometry allow one to select the direction of signal (nematicon in this case) propagation by modifying the amplitude and phase. In particular, we aim to develop efficient methods to form liquid crystalline waveguide structures with the particular spatial distribution of the refractive index within in order to obtain functional elements typical for integrated optics (e.g., waveguides of different shapes, logic gates, Y-junction, switches, and so forth).

Author Contributions: U.A.L. conceived the original idea and wrote the paper. M.K. performed an experimental investigation. All authors have read and agreed to the published version of the manuscript.

Funding: This research was funded by National Centre for Research and Development, grant number LIDER/018/309/L-5/13/NCBR/2014.

Institutional Review Board Statement: Not applicable.

Informed Consent Statement: Not applicable.

Data Availability Statement: Not applicable.

Acknowledgments: We thank P. Jung (Warsaw University of Technology, Warsaw, Poland; University of Central Florida, Orlando, FL, USA) for his help in making the numerical calculations.

Conflicts of Interest: The authors declare no conflict of interest.

References

1. Tong, X.C. Electro-Optic Waveguides. In *Advanced Materials for Integrated Optical Waveguides*; Springer Series in Advanced Microelectronics; Springer International Publishing: Cham, Switzerland, 2014; Volume 46.
2. Courjal, N.; Bernal, M.; Caspar, A.; Ulliac, G.; Bassignot, F.; Gauthier-Manuel, L.; Suarez, M. Lithium Niobate Optical Waveguides and Microwaveguides. In *Emerging Waveguide Technology*; IntechOpen: London, UK, 2018. [CrossRef]
3. Findakly, T.; Suchoski, P.; Leonberger, F. High-quality LiTaO3 integrated-optical waveguides and devices fabricated by the annealed-proton-exchange technique. *Opt. Lett.* **1988**, *13*, 797–798. [CrossRef]
4. Eltes, F.; Caimi, D.; Fallegger, F.; Sousa, M.; O'Connor, E.; Rossell, M.D.; Offrein, B.; Fompeyrine, J.; Abel, S. Low-loss $BaTiO_3$–Si waveguides for nonlinear integrated photonics. *Acs Photonics* **2016**, *3*, 1698–1703. [CrossRef]
5. Qiu, F.; Spring, A.M.; Maeda, D.; Ozawa, M.A.; Odoi, K.; Otomo, A.; Aoki, I.; Yokoyama, S. A hybrid electro-optic polymer and TiO_2 double-slot waveguide modulator. *Sci. Rep.* **2015**, *5*, 8561. [CrossRef] [PubMed]
6. Kabanova, O.S.; Melnikova, E.A.; Olenskaya, I.I.; Tolstik, A.L. Electrically controlled waveguide liquid-crystal elements. *Tech. Phys. Lett.* **2014**, *40*, 598–600. [CrossRef]

7. Asquini, R.; Fratalocchi, A.; d'Alessandro, A.; Assanto, G. Electro-optic routing in a nematic liquid-crystal waveguide. *Appl. Opt.* **2005**, *44*, 4136–4143. [CrossRef] [PubMed]
8. Tabiryan, N.V.; Nersisyan, S.R. Large-angle beam steering using all-optical liquid crystal spatial light modulators. *Appl. Phys. Lett.* **2004**, *84*, 5145–5147. [CrossRef]
9. Yamaguchi, R.; Nose, T.; Sato, S. Liquid Crystal Polarizers with Axially Symmetrical Properties. *Jpn. J. Appl. Phys.* **1989**, *28*, 1730. [CrossRef]
10. Sirleto, L.; Coppola, G.; Breglio, G. Optical multimode interference router based on a liquid crystal waveguide. *J. Opt. A Pure Appl. Opt.* **2003**, *5*, S298. [CrossRef]
11. d'Alessandro, A.; Martini, L.; Civita, L.; Beccherelli, R.; Asquini, R. Liquid crystal waveguide technologies for a new generation of low-power photonic integrated circuits. In Proceedings of the Emerging Liquid Crystal Technologies X, San Francisco, CA, USA, 7–12 February 2015. [CrossRef]
12. Ntogari, G.; Tsipouridou, D.; Kriezis, E.E. A numerical study of optical switches and modulators based on ferroelectric liquid crystals. *J. Opt. A Pure Appl. Opt.* **2005**, *7*, 82. [CrossRef]
13. Costache, F.; Blasl, M. Optical switching with isotropic liquid crystals. *Opt. Photonik* **2011**, *6*, 29–31. [CrossRef]
14. Komar, A.A.; Tolstik, A.L.; Melnikova, E.A.; Muravsky, A.A. Optical switch based on the electrically controlled liquid crystal interface. *Appl. Opt.* **2015**, *54*, 5130–5135. [CrossRef] [PubMed]
15. Khoo, I.C. *Liquid Crystals: Physical Properties and Nonlinear Optical Phenomena*; Wiley: New York, NY, USA, 1995.
16. Peccianti, M.; De Rossi, A.; Assanto, G. Electrically assisted self-confinement and waveguiding in planar nematic liquid crystal cells. *Appl. Phys. Lett.* **2000**, *77*, 7–9. [CrossRef]
17. Beeckman, J.; Neyts, K.; Haelterman, M. Patterned electrode steering of nematicons. *J. Opt. A Pure Appl. Opt.* **2006**, *8*, 214–220. [CrossRef]
18. Assanto, G.; Peccianti, M.; Conti, C. Nematicons: Optical Spatial Solitons in Nematic Liquid Crystals. *Opt. Photonics News* **2003**, *14*, 44–48. [CrossRef]
19. Piccardi, A.; Alberucci, A.; Assanto, G. Nematicons and Their Electro-Optic Control: Light Localization and Signal Readdressing via Reorientation in Liquid Crystals. *Int. J. Mol. Sci.* **2013**, *14*, 19932–19950. [CrossRef]
20. Assanto, G. Nematicons: Reorientational solitons from optics to photonics. *Liq. Cryst. Rev.* **2018**, *6*, 170–194. [CrossRef]
21. Peccianti, M.; Conti, C.; Assanto, G. All-optical switching and logic gating with spatial solitons in liquid crystals. *Appl. Phys. Lett.* **2002**, *81*, 3335–3337. [CrossRef]
22. Peccianti, M.; Assanto, G. Signal readdressing by steering of spatial solitons in bulk nematic liquid crystals. *Opt. Lett.* **2001**, *26*, 1690–1692. [CrossRef]
23. Laudyn, U.A.; Piccardi, A.; Kwasny, M.; Karpierz, M.A.; Assanto, G. Thermo-optic soliton routing in nematic liquid crystals. *Opt. Lett.* **2018**, *43*, 2296–2299. [CrossRef]
24. Laudyn, U.A.; Piccardi, A.; Kwasny, M.; Klus, B.; Karpierz, M.A.; Assanto, G. Interplay of Thermo-Optic and Reorientational Responses in Nematicon Generation. *Materials* **2018**, *11*, 1837. [CrossRef]
25. Laudyn, U.A.; Kwaśny, M.; Karpierz, M.A.; Smyth, N.F.; Assanto, G. Accelerated optical solitons in reorientational media with transverse invariance and longitudinally modulated birefringence. *Phys. Rev. A* **2018**, *98*, 023810. [CrossRef]
26. Laudyn, U.A.; Kwaśny, M.; Sala, F.A.; Karpierz, M.A.; Smyth, N.F.; Assanto, G. Curved optical solitons subject to transverse acceleration in reorientational soft matter. *Sci. Rep.* **2017**, *7*, 12385. [CrossRef]
27. Dąbrowski, R. New Liquid Crystalline Materials for Photonic Applications. *Mol. Cryst. Liq. Cryst.* **2004**, *421*, 1–21. [CrossRef]
28. Kim, Y.; Lee, M.; Wang, H.S.; Song, K. The effect of surface polarity of glass on liquid crystal alignment. *Liq. Cryst.* **2018**, *45*, 757–764. [CrossRef]
29. Komar, A.A.; Kurochkina, M.A.; Melnikova, A.A.; Stankevich, A.I.; Tolstik, A.L. Polarization separation of light beams at the interface of two mesophases. *Tech. Phys. Lett.* **2011**, *37*, 704. [CrossRef]
30. Barboza, R.; Alberucci, A.; Assanto, G. Large electro-optic beam steering with nematicons. *Opt. Lett.* **2011**, *36*, 2725–2727. [CrossRef]
31. Kazak, A.A.; Melnikova, E.A.; Tolstik, A.L.; Mahilny, U.V.; Stankevich, A.I. Controlled diffraction liquid-crystal structures with a photoalignment polymer. *Tech. Phys. Lett.* **2008**, *34*, 861–863. [CrossRef]
32. Kazak, A.A.; Tolstik, A.L.; Mel'nikova, E.A. Controlling light fields by means of liquid-crystal diffraction elements. *J. Opt. Technol.* **2010**, *77*, 461–462. [CrossRef]
33. Sarkissian, H.; Serak, S.V.; Tabiryan, N.V.; Glebov, L.B.; Rotar, V.; Zeldovich, B.Y. Polarization-controlled switching between diffraction orders in transverse-periodically aligned nematic liquid crystals. *Opt. Lett.* **2006**, *31*, 2248–2250. [CrossRef]